How to cite: *Angew. Chem. Int. Ed.* **2023**, *62*, e202306654
doi.org/10.1002/anie.202306654

Magnetic Resonance Imaging

In Vivo Metabolic Imaging of [1-^{13}C]Pyruvate-d$_3$ Hyperpolarized By Reversible Exchange With Parahydrogen**

Henri de Maissin[#], Philipp R. Groß[#], Obaid Mohiuddin[#], Moritz Weigt[#], Luca Nagel, Marvin Herzog, Zirun Wang, Robert Willing, Wilfried Reichardt, Martin Pichotka, Lisa Heß, Thomas Reinheckel, Henning J. Jessen, Robert Zeiser, Michael Bock, Dominik von Elverfeldt, Maxim Zaitsev, Sergey Korchak, Stefan Glöggler, Jan-Bernd Hövener, Eduard Y. Chekmenev, Franz Schilling, Stephan Knecht, and Andreas B. Schmidt**

Abstract: Metabolic magnetic resonance imaging (MRI) using hyperpolarized (HP) pyruvate is becoming a non-invasive technique for diagnosing, staging, and monitoring response to treatment in cancer and other diseases. The clinically established method for producing HP pyruvate, dissolution dynamic nuclear polarization, however, is rather complex and slow. Signal Amplification By Reversible Exchange (SABRE) is an ultra-fast and low-cost method based on fast chemical exchange. Here, for the first time, we demonstrate not only in vivo utility, but also metabolic MRI with SABRE. We present a novel routine to produce aqueous HP [1-^{13}C]pyruvate-d$_3$ for injection in 6 minutes. The injected solution was sterile, non-toxic, pH neutral and contained ≈30 mM [1-^{13}C]pyruvate-d$_3$ polarized to ≈11 % (residual 250 mM methanol and 20 μM catalyst). It was obtained by rapid solvent evaporation and metal filtering, which we detail in this manuscript. This achievement makes HP pyruvate MRI available to a wide biomedical community for fast metabolic imaging of living organisms.

[*] H. de Maissin,[#] P. R. Groß,[#] O. Mohiuddin,[#] Dr. M. Weigt,[#] M. Herzog, Z. Wang, R. Willing, Dr. W. Reichardt, Dr. M. Pichotka, Prof. Dr. M. Bock, Prof. D. von Elverfeldt, Prof. Dr. M. Zaitsev, Dr. A. B. Schmidt
Division of Medical Physics, Department of Radiology, Medical Center, Faculty of Medicine, University of Freiburg
Killianstr. 5a, 79106 Freiburg (Germany)
E-mail: andreas.schmidt@uniklinik-freiburg.de

H. de Maissin,[#] R. Willing, Prof. Dr. T. Reinheckel, Prof. Dr. R. Zeiser, Dr. A. B. Schmidt
German Cancer Consortium (DKTK), partner site Freiburg and German Cancer Research Center (DKFZ)
Im Neuenheimer Feld 280, 69120 Heidelberg (Germany)

L. Nagel, Prof. Dr. F. Schilling
Department of Nuclear Medicine, Klinikum rechts der Isar, Technical University of Munich
Ismaninger Str. 22, 81675 Munich (Germany)

Dr. L. Heß, Prof. Dr. T. Reinheckel
Institute of Molecular Medicine and Cell Research, Faculty of Medicine, University of Freiburg
Stefan-Meier-Str. 17, 79104 Freiburg (Germany)

Prof. Dr. H. J. Jessen
Bioorganic Chemistry, Institute of Organic Chemistry, Albert-Ludwigs-University of Freiburg
Albertstrasse 21, 79104 Freiburg (Germany)

Prof. Dr. R. Zeiser
Hematology and Oncology, Department of Medicine I, Medical Center, Faculty of Medicine, University of Freiburg
Hugstetter Strasse 55, 79106 Freiburg (Germany)

Dr. S. Korchak, Dr. S. Glöggler
NMR Signal Enhancement Group, Max Planck Institute for Multidisciplinary Sciences
Am Fassberg 11, 37077 Göttingen (Germany)

Dr. S. Korchak, Dr. S. Glöggler
Center for Biostructural Imaging of Neurodegeneration of the University Medical Center Göttingen
Von-Siebold-Str. 3 A, 37075 Göttigen (Germany)

Prof. Dr. J.-B. Hövener
Section Biomedical Imaging SBMI, Molecular Imaging North Competence Center MOINCC, Department of Radiology and Neuroradiology, University Hospital Schleswig-Holstein, Kiel University
24105 Kiel (Germany)

Prof. Dr. E. Y. Chekmenev, Dr. A. B. Schmidt
Department of Chemistry, Integrative Biosciences (Ibio), Karmanos CancerInstitute (KCI), Wayne State University
Detroit, MI 48202 (USA)

Prof. Dr. F. Schilling
German Cancer Consortium (DKTK), partner site Munich and German Cancer Research Center (DKFZ)
Im Neuenheimer Feld 280, 69120 Heidelberg (Germany)

Dr. S. Knecht
NVision Imaging Technologies GmbH
89081 Ulm (Germany)
E-mail: stephan@nvision-imaging.com

[#] Co-first authors.

[**] A previous version of this manuscript has been deposited on a preprint server (https://doi.org/10.26434/chemrxiv-2023-9trxb).

Introduction

Non-invasive imaging techniques such as Computed Tomography (CT) and Magnetic Resonance Imaging (MRI) are widely used in oncology for characterizing tumors before treatment, therapy planning, monitoring tumor progression, evaluating treatment response, and follow-up. Most clinical guidelines rely on morphological criteria such as size and location of the tumor, e.g. RECIST criteria.[1] However, many effective therapies, including promising immunotherapies, do not manifest early morphological changes such as tumor size reduction, even if the patient responds well to treatment.[2] The current advances in molecular tumor biology, genetics, and imaging technology have led to a major paradigm shift in oncology to utilize molecular imaging as a superior diagnostic and prognostic marker of cancer staging, response to treatment and survival. [^{18}F]Fluorodeoxyglucose (FDG) Positron Emission Tomography (FDG PET) is the most widely clinically applied molecular imaging technique that reports on aberrant energy metabolism, which is a hallmark of many cancers. Despite limitations (including long examination times >1 h and the use of ionizing radiation), this radioactive tracer has revolutionized treatment and management of many cancers. Its success relies on the FDG uptake, which is elevated in proliferating tumors. However, PET is not able to distinguish between metabolic products. Non-radioactive molecular contrast agents providing deeper insights in aberrant metabolism with faster scan time are needed. Hyperpolarized (HP) [1-^{13}C]pyruvate MRI has shown great promise for non-invasive, non-ionizing molecular imaging, e.g. for tumor grading or therapy response assessment.[3–6] Such molecular MRI scan takes about one minute and employs non-ionizing radiation. As a result, it has been embraced as a next-generation molecular imaging modality. Similarly to FDG, pyruvate is a key metabolite at the cross-section of cellular energy pathways. The high acquisition speed of HP pyruvate MRI builds on the ability to visualize (and distinguish) the conversion of metabolites into downstream products in vivo, which mitigates the requirement for contrast agent clearance from the surrounding tissues. Since the first demonstration in human 2013, HP [1-^{13}C]pyruvate MRI has made a remarkable progress, and this technique is currently being investigated in over 30 clinical trials according to clinicaltrials.gov. Moreover, the United States Food and Drug Administration (FDA) has recently approved HP ^{129}Xe gas for ventilation lung imaging. Following this landmark regulatory decision, it is anticipated that HP [1-^{13}C]pyruvate may also soon be approved for the use in oncology.

The success of HP [1-^{13}C]pyruvate MRI was enabled by dissolution Dynamic Nuclear Polarization (dDNP), which is the leading technique for producing HP pyruvate.[7] While this polarization method is developing rapidly and great improvements have been presented in recent years,[8–10] instrumentation and HP bolus preparation are still elaborate necessitating superconducting magnets ($>$1T), cryogenic temperatures(<2 K), and microwave irradiation for agent polarization in the solid phase, followed by rapid unfreezing and sample dissolution typically using superheated water to transfer HP metabolites in the liquid aqueous phase. Also, current dDNP requires about one hour to produce a bolus of HP [1-^{13}C]pyruvate (although e.g. ^{1}H–^{13}C cross polarization promises to cut this time[10]). Hence, faster, less expensive, and simpler technologies are desirable to improve access of the biomedical community to this promising molecular contrast agent.

Parahydrogen-induced polarization (PHIP) techniques have emerged as promising candidates to address this need for efficient polarization methods.[11–14] PHIP utilizes the nuclear spin singlet isomer of molecular hydrogen, parahydrogen (pH_2), which acts as a cost-efficient source of hyperpolarization. In contrast to DNP, PHIP does not require cryogenic temperatures nor strong magnetic fields, but relies on pH_2 and chemical reactions instead. These properties make PHIP intrinsically less complex and less expensive than DNP. One way to exploit this source of spin order relies on rapid permanent addition of pH_2, i.e., hydrogenation of an unsaturated precursor molecule—a method often referred to as hydrogenative PHIP that is known since the 1980s and has recently been enabled for pyruvate by Side-Arm Hydrogenation (PHIP-SAH) of a pyruvate ester by Reineri et al.[15] In 2009, a "non-hydrogenative" PHIP approach called Signal Amplification By Reversible Exchange (SABRE) has been pioneered by Duckett and co-workers.[16] SABRE is based on the reversible, simultaneous chemical exchange of pH_2 and the target to-be-hyperpolarized molecule to an iridium-based exchange complex, such that hyperpolarization derived from pH_2 is transferred to a substrate nucleus.[17–22] In 2019, Duckett et al. demonstrated the production of HP [1-^{13}C]pyruvate-h_3 via SABRE by doping the catalyst with a dimethyl sulfoxide (DMSO) co-ligand to improve the binding properties of pyruvate acting as a bidentate ligand (Figure 1a).[23] This breakthrough has garnered significant interest in utilizing SABRE HP pyruvate for metabolic imaging studies.[24–27] However, the SABRE technique typically employs organic solvents such as methanol for the hyperpolarization process, rendering the produced HP [1-^{13}C]pyruvate too toxic for in vivo administration. Previous studies have shown that the direct SABRE polarization in biocompatible solvents like aqueous media is significantly lower (by an order of magnitude or more) compared to that in methanol. This decrease in polarization is likely due to lower hydrogen solubility and other contributing factors.[28–30] Moreover, as SABRE hyperpolarization requires iridium-based catalysts, removal of residual iridium (Ir, below 1 ppm or less) in the injectable solution is required for biocompatible formulations. Metal scavenging approaches have demonstrated reducing the Ir concentration, but have not allowed the production of hyperpolarized [1-^{13}C]pyruvate, nor eliminated the need for methanol.[31,32]

Recently, we have presented a method based on pyruvate precipitation and a phase separation approach that reduced both toxic solvent and Ir in SABRE HP pyruvate solutions. However, that approach still suffered from high methanol content ($\approx$5 M), low pyruvate concentration ($\approx$6 mM), and 44 μM Ir in the final solutions.[27] Consequently, to date, there are no peer-reviewed studies that

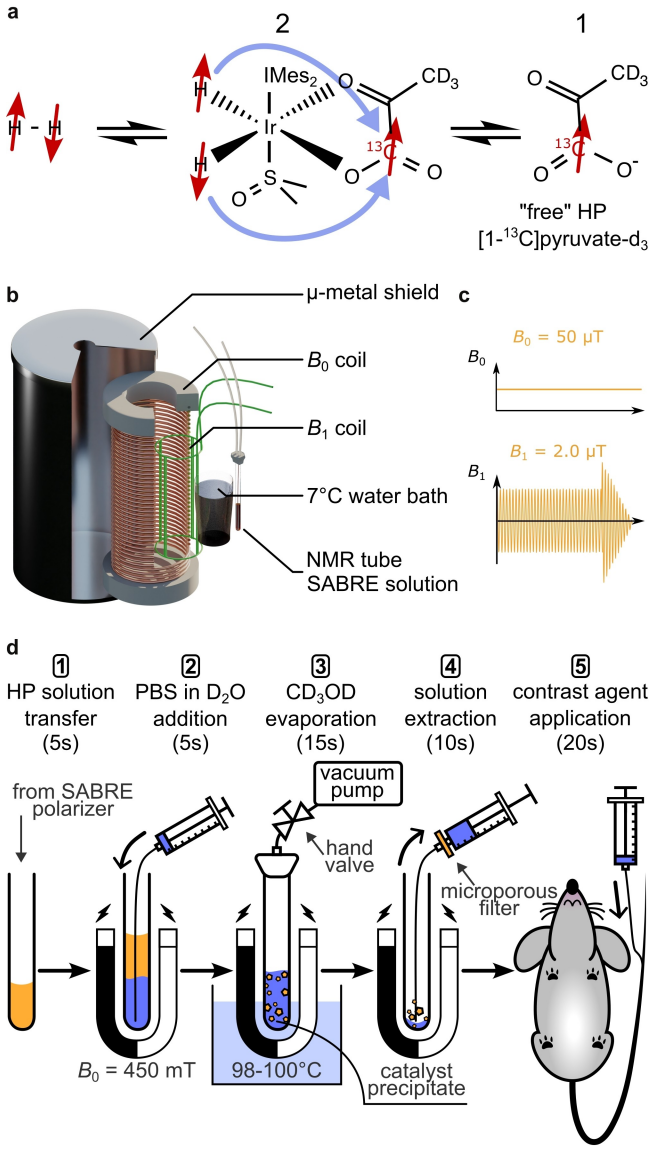

Figure 1. Process of SLIC-SABRE hyperpolarization and purification of [1-^{13}C]pyruvate-d$_3$ samples. a, schematic representation of the SABRE hyperpolarization reaction involving the binding of pH_2 and [1-^{13}C]pyruvate-d$_3$ to the SABRE catalyst for polarization transfer to pyruvate. b, experimental setup for the SLIC-SABRE method, which includes the static magnetic field B_0, radiofrequency field B_1, NMR tube bubbling system to introduce pH_2 to pyruvate in methanol-d$_4$, and a mu-metal to shield external fields. c, during SLIC-SABRE, B_0 was set constant at 50 μT, and the B_1 amplitude was set to 2 μT. After the SLIC pulse, an adiabatic pulse was applied. d, stepwise purification and application protocol consisting of buffered-D_2O addition, solvent evaporation under vacuum in a hot water bath, solution filtering, and in vivo administration. More details on the experiment are presented in the SI.

report on satisfyingly-clean solutions with satisfyingly-high polarization levels of SABRE-polarized pyruvate, let alone an in vivo application or metabolic imaging.

In the present paper, we address these SABRE translational challenges and demonstrate, for the first time, metabolic imaging with SABRE in healthy mice, using purified SABRE-polarized pyruvate. These results were enabled by developing a fast physico-chemical process including spin-lock induced crossing (SLIC) SABRE[33,34] at microtesla fields (Figure 1b–c),[35,36] providing up to ≈16 % ^{13}C polarization of [1-^{13}C]pyruvate-d$_3$. We achieved rapid purification by solvent evaporation and metal filtration, reducing methanol and catalyst below acute toxic levels (Figure 1d). Tail-vein administration of the agent and chemical shift imaging of pyruvate metabolic conversion enabled metabolic mapping of downstream HP lactate and alanine, demonstrating the translational promise of this technique. All animals tolerated the injections well.

Results and Discussion

Efficient SABRE Hyperpolarization

We obtained mean ^{13}C polarizations for [1-^{13}C]pyruvate-d$_3$ of 13±3 % (N=5 samples, each hyperpolarized and polarization quantified three times before purification) with a maximum of 16.3 % at the time of detection (5–8 s after production) in methanol-d$_4$ using the setup and protocol described in the Supporting Information (Figure 2a and Figure 2b). Note that the polarization at thermal equilibrium at 1T is only 0.000086 %. The high polarization levels were made possible by the long relaxation times during the SLIC-SABRE polarization process of $T_{1\rho}$=113.3±0.3 s (Figure 2c), which allowed for effective polarization buildup over a 5-minute period (see Supporting Information Figure S5).[36]

Fast Purification

Encouraged by these high polarization levels, and inspired by a recent study by Ding et al.,[37] we investigated the removal of methanol from the samples by rapid solvent evaporation. As methanol and water do not form an azeotrope and hence evaporate at separate boiling points, we added phosphate-buffered D_2O to the HP SABRE sample in an NMR tube and placed the mixture in a hot water bath while applying vacuum (≈5 mbar, Figure 1d). Strikingly, we found that evacuating the sample for 15 seconds at 98 °C reduced methanol from 24.75 M to 250 mM while retaining ≈30 mM of the pyruvate in the resulting ≈150 μL aqueous solution (Figure 2d and Figs. S7 and S11). Although a longer evaporation period increased the pyruvate concentration (SI Figure S12), water was lost at the same time, too, so that the volume was too little for injection.

To reduce polarization losses during the purification procedure, which consisted of 15 seconds of vacuum and approximately 40 s of sample handling (including filtering the solution through a 1.2 μm microporous syringe filter), the procedure was mostly conducted at an elevated magnetic field of ≈450 mT. Additionally, we retained the pyruvate in phosphate-buffered D_2O instead of phosphate-buffered H_2O, which features shorter lifetimes throughout the

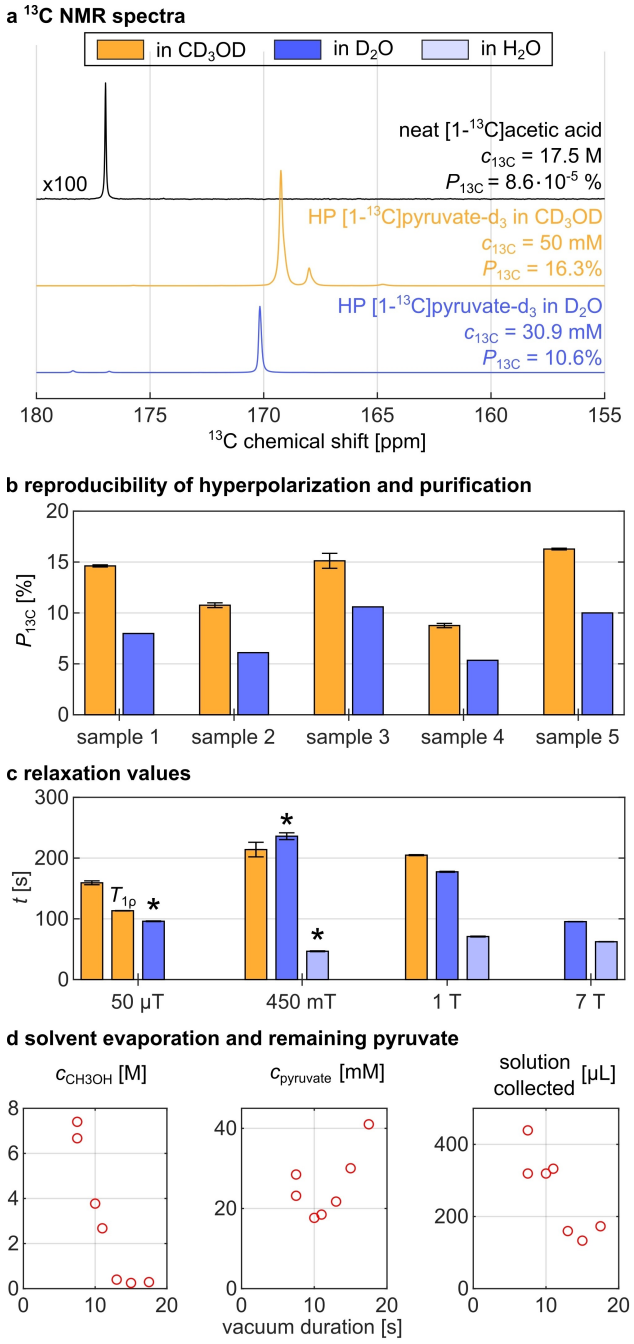

Figure 2. SABRE hyperpolarization and purification of [1-^{13}C]pyruvate-d$_3$. a, ^{13}C NMR spectra of [1-^{13}C]pyruvate-d$_3$ in methanol-d$_4$ before (orange) and in pH-buffered D_2O after purification (blue) compared with an external ^{13}C-enriched reference solution (black) at 1 T. b, reproducibility of SLIC-SABRE hyperpolarization and purification investigated in 5 independent samples. c, longitudinal relaxation times T_1 and $T_{1\rho}$ in presence of the SLIC pulse at different fields in methanol-d$_4$ (orange), phosphate-buffered D_2O (blue), and phosphate-buffered H_2O (light blue). *these data were acquired in thermally polarized samples, see SI. d, remaining concentrations of methanol and pyruvate after applying vacuum and a 98 °C water bath for different amount of time to a 600 µL sample of SABRE solution (including 50 mM sodium pyruvate in 24.75 M methanol) mixed with 600 µL phosphate-buffered D_2O (see Supporting Information Figure S7 and S11). The error bars in b represent the standard deviation obtained from three measurements of the corresponding sample. The error bars in c correspond to the error of the fitted exponential curves (see SI).

investigated fields (Figure 2c). Using this approach, we reproducibly obtained a factor of 0.60 ± 0.07 of the initial ^{13}C polarization of the unpurified sample (mean and standard deviation of $N = 5$ independent samples), and the final ≈ 30 mM pyruvate in the extracted samples were polarized up to ≈ 11 % (Figure 2b). This highly optimized, accelerated and spin-order preserving reaction Scheme allowed us to obtain a dose of freshly purified pyruvate, ready for injection, in 6 min only.

Aqueous Sample Analysis

After reducing the methanol content to ≈ 250 mM, the catalyst visibly precipitated from the solution. As an additional measure, the solution was passed through a 1.2 µm filter, effectively removing the precipitated catalyst and resulting in a clear solution (SI Figure S9). During the in vivo experiments, we found these two visual inspections of the sample, one before and one after filtering, helpful to determine whether methanol and catalyst were successfully reduced.

We used inductively coupled plasma optical emission spectroscopy (ICP-OES) to quantify the remaining iridium content in the samples, which showed successful reduction from 6 mM to 20 µM, i.e. to < 0.5 ppm after purification. Directly before administration, we measured the temperature of the solutions to be 35 ± 2 °C.

We tested the purified solutions to evaluate if they are suitable for in vivo applications. Our analysis indicated that the resulting aqueous solutions were sterile (see Supporting Information Figure S13) and had neutral pH and osmolarity (see Supporting Information Figure S10). Cytotoxicity assays showed no adverse effects on cell viability when exposed to the purified SABRE pyruvate solutions at concentrations reached in the bloodstream after in vivo injection and even at a twofold higher concentration. A toxicity observed at a 10-times higher concentration was likely caused by the residual catalyst and high concentration of pyruvate (see Supporting Information Figure S14).

In Vivo Metabolic Imaging

To demonstrate that our purified SLIC-SABRE [1-^{13}C]pyruvate-d$_3$ is suitable for in vivo metabolic imaging, we performed first experiments on healthy mice using a dedicated mouse quadrature resonator and a 7 T preclinical MRI system. To obtain high ^{13}C signal in vivo, we decided to use an HP sample only if polarization prior purification was ≥ 15 % and if the purified sample volume was ≈ 150 µL (production time ≈ 6 min per dose). All ^{13}C images were obtained after injection of a single bolus of up to 5 µL/g of an HP pyruvate solution through the tail vein. 15 s after starting administration, we applied a center-out phase encoded ^{13}C Chemical Shift Imaging (CSI) sequence with 12° flip angle from a 3-mm axial slice covering the kidneys and parts of the liver and gut (Figure 3). Strong HP ^{13}C signal of pyruvate and its metabolites was observed, and ^{13}C

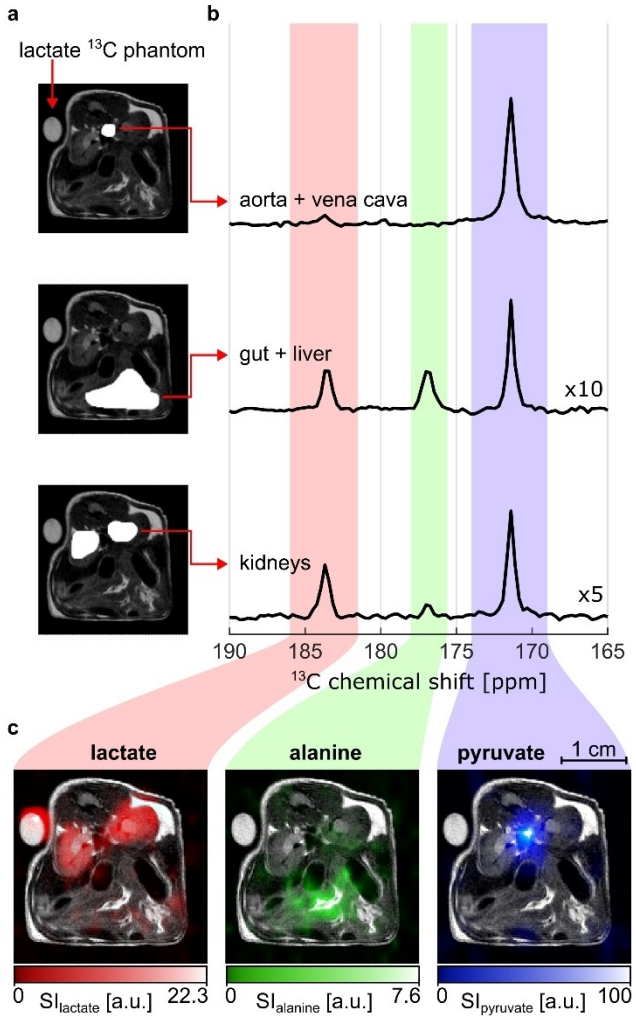

Figure 3. In vivo ^{13}C chemical shift imaging of SABRE-hyperpolarized [1-^{13}C]pyruvate-d_3 acquired starting 15 s after beginning the HP bolus injection. a, anatomical ^{1}H MRI showing regions of interests (white) used to calculate ^{13}C-spectra: aorta and vena cava (top), the gut and liver (middle), and the kidneys (bottom). b, corresponding summated ^{13}C NMR spectra from these regions with metabolite ^{13}C signals from pyruvate (blue), alanine (green), and lactate (red). c, 2D metabolite maps of lactate, alanine, and pyruvate (same colors as in b) superimposed with an anatomical ^{1}H MRI of the same axial slice (^{13}C CSI recorded: 3 mm slice thickness, 20×14 matrix, 1.5×1.5 mm^2 in-plane resolution). The unprocessed ^{13}C MRI data are presented in the SI.

spectra and metabolic maps were reconstructed. The ^{13}C signal of pyruvate was found mainly in the aorta and vena cava. While in the kidney mostly lactate was observed, the liver and gut contained considerable amounts of alanine.

In a second experiment, we tested metabolic imaging with higher spatial and temporal resolution using a fast, metabolite-selective 3D ^{13}C balanced Steady-State Free Precession (bSSFP) sequence.[38] Here, we focused on the pyruvate-to-lactate conversion and started a series of alternated ^{13}C pyruvate and lactate MRI acquisitions approximately 15 s prior to the start of the injection of HP [1-^{13}C]pyruvate-d_3 yielding a temporal resolution of 0.87 Hz (Figure 4). This setting enabled us to monitor the conversion kinetics clearly showing the arrival of the HP pyruvate bolus and the subsequent formation of lactate. From the 3D time-resolved data, we reconstructed images depicting pyruvate that was observed mostly in the heart, aorta and vena cava, and lactate that was formed predominantly in the kidneys.

In total, we performed metabolic MRI in four mice and observed no adverse effects to the injection for the remainder of the MRI investigation (≈20–30 min). During the imaging experiment, we observed only a temporary increase in breathing rate following the injection (see Supporting Information Figure S19). After approximately 1–2 min, the breathing rate returned to pre-injection values and remained stable throughout the experiment. This bolus-induced temporary increase in breathing rate is a commonly observed side effect to the increased volume entering the

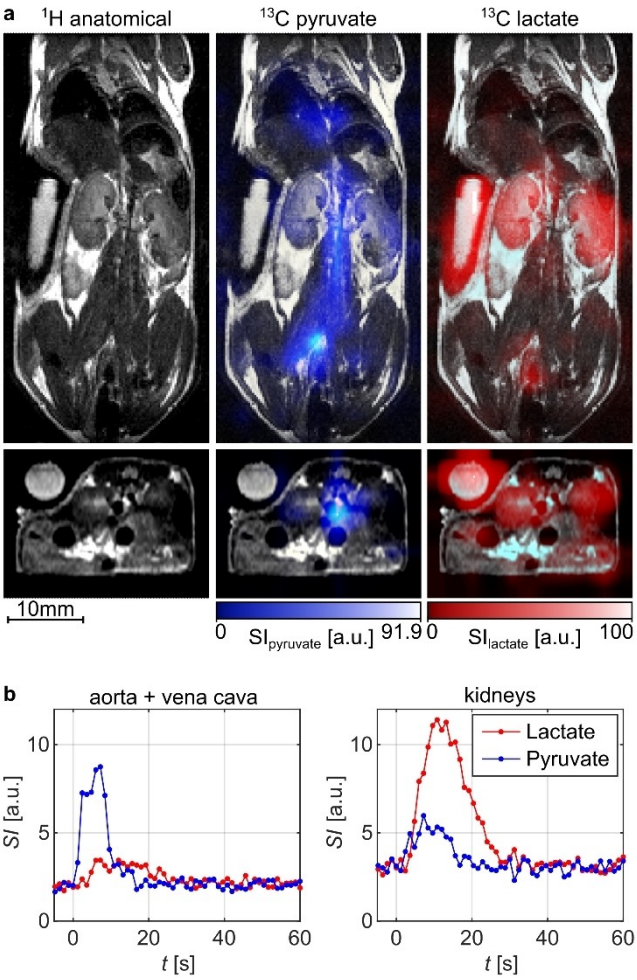

Figure 4. 3D dynamic in vivo ^{13}C metabolic imaging of pyruvate-to-lactate conversion. a, coronal (top) and axial view (bottom) of anatomical ^{1}H MRI (left), superimposed with time-summated ^{13}C-pyruvate (center) and ^{13}C-lactate signal (right). b, metabolite conversion kinetics of pyruvate and lactate located to aorta and vena cava (left) and the kidneys (right). ^{13}C MRI: 21×11×8 matrix, 2.5×2.5×2.5 mm^3 resolution, temporal resolution of≈0.87 Hz. The measurement was started before beginning the injection. The unprocessed data is presented in the SI.

right ventricle and lung circulation. The mice were sacrificed at the end of the imaging experiment.

Overall, the in vivo experiment confirmed that SABRE-polarized pyruvate is well suited for metabolic imaging and demonstrated its power for monitoring metabolic processes in vivo.

Discussion

Here, we present a method for obtaining SABRE-hyperpolarized pyruvate in sterile aqueous media and demonstrate its applicability for in vivo metabolic MRI. To the best of our knowledge, this is the first time that a hyperpolarized, injectable dose of pyruvate was produced within minutes and without conformal changes to the molecule.

Our new SABRE approach was inspired by the previous PHIP-SAH advances for obtaining aqueous HP [1-^{13}C]pyruvate solutions. Both methods use pH_2 spin order and a chemical reaction in organic solvents (often acetone or chloroform for PHIP-SAH and methanol for SABRE) in the presence of a metal-based catalyst (typically rhodium-based for PHIP-SAH and the Ir-IMes exchange catalyst for SABRE). Subsequently polarization is transferred to the target [1-^{13}C] nuclear site and the toxic solution is purified to reduce the organic solvent and catalyst content. Despite substantial differences in chemistry of hyperpolarization, both methods feature a fast polarization build-up process that allows for continuous or quasi-continuous delivery of HP molecules.[39,40] An advantage of SABRE is that no conformal changes to the molecule (pyruvate) are needed—an important aspect when it comes to regulatory considerations (no agent synthesis during the polarization process).[12]

Our SABRE approach currently allows us to polarize a dose of HP pyruvate in about six minutes or several doses during one imaging session (i.e., in the duration of one anesthesia). The fundamental difference between the two methods lies in the incorporation of the pH_2 spin order: SABRE utilizes reversible temporary binding of pH_2 and pyruvate to the catalyst while PHIP-SAH uses permanent pairwise addition by hydrogenation with pH_2. To enable the "hydrogenative" PHIP approach, side-arm hydrogenation is utilized as pyruvate lacks a direct unsaturated precursor. Hence, this method requires the synthesis of appropriate esterified precursors for the permanent addition of pH_2.[11,12] As a consequence, the purification for PHIP-SAH typically includes fast cleavage of the ester side-arm to receive the HP pyruvate.[15] Here we used isotope-enriched [1-^{13}C]pyruvate-d_3, which is available commercially and requires no further chemical modification for SABRE hyperpolarization. The commercial availability of the substrate and elimination of the side-arm cleavage step during purification are promising advantages.

We chose to use the deuterated pyruvate isotopologue for our studies, as our recent research has shown approximately twice the polarization compared to the protonated form. Furthermore, we observed longer ^{13}C T_1 relaxation times for pyruvate-d_3 compared to pyruvate-h_3 in our previous study (approximately 220 s versus approximately 140 s at 1.9 T, respectively), which we deemed beneficial to maximize the ^{13}C polarization levels after the approximately 1-minute purification process.[36] It is noteworthy that the metabolic conversion kinetics of pyruvate is not affected by the presence of deuterium isotopes, as evidenced by previous studies.[41] Therefore, for metabolic HP MRI, pyruvate-d_3 can be utilized successfully in place of non-deuterated pyruvate.

Here, we observed a reduction in polarization during the purification process to a factor of 0.60 ± 0.07. Most of this loss can be attributed to longitudinal relaxation: given the measured T_1 values at 450 mT, we would expect a reduction factor of ≈ 0.75. Additional losses may have been caused by factors such as T_1 changes at higher temperatures, shorter T_1 during transfer and handling at lower magnetic fields, and potential relaxation by the precipitated Ir catalyst during and after solvent removal. These aspects need to be further investigated—subject to our ongoing systematic studies. While faster sample handling and purification would minimize polarization losses, we were already able to achieve a high enough signal-to-noise ratio for in vivo monitoring of pyruvate metabolism in mice using ^{13}C MRI.

While we have achieved this significant breakthrough, there are still limitations to our current method. One such limitation is the observed large inter-sample polarization deviations, with a mean ^{13}C polarization of 13 ± 3 %. This deviation is similar to that seen in previous studies, such as 8 ± 2 %[27] and 10 ± 1 %[24] for 30 mM [1-^{13}C]pyruvate-h_3 in methanol with SABRE SHEATH. For the latest generation preclinical DNP device, a 15 % coefficient of variation was reported for ^{13}C-pyruvate.[42] The origin of this variability is currently speculative, but we believe that experimental variations such as different sample positions in the SLIC-SABRE setup, impurities from previous experiments, and positioning of the bubbling catheter leading to different pH_2 gas to solvent surface areas may be contributing factors. These effects should be further investigated to improve the consistency and reproducibility of our method. Other limitations of our current method are (a) the extracted volume and (b) the pyruvate concentration, which are ≈ 150 µL and ≈ 30 mM, respectively. These measures are sufficient for in vivo mouse studies, but larger amounts are necessary e.g. for rat or large animal measurements. Currently, the size of our experimental setup is the limiting factor for producing larger doses, for which we see no fundamental hurdles. Scaling up the reaction vessels, tubes, B_0 and B_1 coils and the µ-metal shield is expected to provide larger volumes. Once higher volumes are produced, the pyruvate concentration can be increased further by prolonging the evaporation period, as we have shown already (Figure S12). Another approach would be to increase the initial concentration of pyruvate, although to achieve efficient SABRE polarization, the pH_2 concentration in methanol would also need to be increased, for example, by applying higher pressure.[24,43] Therefore, dedicated high-pressure reactors would need to be developed in the future to enable the desired injection volume and minimize solution losses.[44,45]

The purification scheme proposed here is fast and easy to install, reducing both methanol and catalyst below acute toxic levels. Hence, we foresee this technique being available to many researchers. In future, a faster and more complete evaporation of methanol may be accomplished through optimizing vacuum and temperature, using larger evaporation chambers, and increasing the surface area between the liquid and gas phases. Note that reducing the methanol content may also result in a further decrease in the current levels of iridium. It is important to consider that our specific approach capitalizes on the low solubility of the used catalyst in water, causing it to precipitate when methanol is evaporated. As a result, our proposed purification method may not be suitable to reduce catalyst for SABRE approaches that seek to generate polarization directly in aqueous media using water-soluble catalysts.[28–30]

Finally, we want to consider the current levels of residual methanol and catalyst in the purified samples. Our current purification scheme results in a methanol concentration of approximately 12.5 mM or 400 mg/L in the bloodstream of injected mice, equivalent to 40 mg/kg of methanol per mouse weight. Already now, this concentration is well below the reported oral LD50 (5.628 g/kg) and LD00 (143 mg/kg) values for rodents,[46] and close to the threshold beyond which humans get treated after methanol poisoning (300 mg/L blood).[47] With regard to the SABRE catalyst, we were unable to identify toxicity studies in the literature. However, our tests have shown toxicity to cells only at concentrations higher than the final concentration found in the bloodstream. For preclinical and, possibly at some point in the future, clinical applications, several factors have to be considered. With respect to methanol and iridium, the international council for harmonization (ICH) guidelines suggest acceptable amounts of 3,000 ppm of methanol and 10 μg Ir.[48,49] Compared to what is achieved here, in this first demonstration, the methanol content would need to be reduced at least 3-fold and the Iridium content at least 20-fold (see SI). The current levels may allow conducting first preclinical studies, but more actions will be needed to reach concentrations acceptable for human application. Hence, we will continue to work towards reducing them in the future.

Conclusion

In conclusion, our study demonstrates that non-invasive in vivo metabolic imaging is feasible with SABRE hyperpolarized pyruvate, produced in aqueous solution. The entailed bioburden appears to be low, whereas the production process is much faster (< 10 min) and relatively simple to install compared to a dDNP experiment.

The efficient hyperpolarization of pyruvate and its translation to preclinical imaging have been a major focus of SABRE research since its discovery in 2009. In this study, we successfully hyperpolarized [1-^{13}C]pyruvate-d_3 using SLIC-SABRE at microtesla field,[36] and the long-lived polarization allowed us to extract highly-hyperpolarized [1-^{13}C]pyruvate-d_3 in purified aqueous solutions. This approach enabled us to conduct the first in vivo metabolic MRI with SABRE hyperpolarized pyruvate. We also note that further multi-site validation is provided by a group from North Carolina State University that was able to provide first in vivo data using SABRE-polarized pyruvate at the same time.[56] This is a promising accomplishment, given that pyruvate is the most widely applied HP MRI agent.

Our results demonstrate that SABRE is now a viable option for preclinical metabolic pyruvate MRI, with a sufficiently high signal-to-noise ratio to monitor pyruvate metabolism in mice accurately. We envision this technique to be widely adopted by researchers, paving the way for improved metabolic imaging and a better understanding of metabolic changes in cancer and other pathologies.

Supporting Information

Please find additional experimental details, and sample characterization, MRI, and relaxation data in the Supporting Information file. The authors have cited additional references within the SI.[50–55]

Acknowledgements

Research reported in this publication was supported by the German Federal Ministry of Education and Research (BMBF) in the funding program "Quantum Technologies—from Basic Research to Market" under the project "QuE-MRT" (contract number: 13N16448), the German Cancer Consortium (DKTK), B.E.S.T. Fluidsysteme GmbH I Swagelok Stuttgart, and the German Research Foundation (DFG #SCHM 3694/1-1, #SCHM 3694/2–1, #SFB1479 Project ID: 441891347SFB1160, #423813989/GRK2606). ABS and MP thank the Research Commission of the University Medical Center Freiburg for support. EYC thanks NSF CHE-1904780. ABS and EYC thank Wayne State University for a Postdoctoral Fellow award. JBH acknowledges support by the DFG, BMBF BlueHealthTech and the medical faculty of Kiel University (HO-4602/2, HO-4602/3, EXC2167, FOR5042, 03WIR6208 A). FS received support from the DFG (#391523415) and the Young Academy of the Bavarian Academy of Sciences and Humanities. EU Proposal n° ERC-2022-ADG Project: 101094168—AlloCure (ERC Advanced grant to RZ). The authors thank the 'Preclinical Imaging Research Center - Core Facility' (AMIR^{CF}; DFG-RIsources N° RI_00052) and the Freiburg MagRes union for support in data acquisition. Open Access funding enabled and organized by Projekt DEAL.

Conflict of Interest

SK is an employee of NVision Imaging Technologies GmbH. FS serves on the scientific advisory board of NVision Imaging Technologies GmbH. EYC holds a stake of ownership in XeUS Technologies Ltd. and serves on the scientific advisory board of Visma Life Sciences LLC. SK and SG are co-founders of MagniKeen, a spin-off of the

Max Planck Institute for Multidisciplinary Natural Sciences, Göttingen. The other authors have no competing interests to declare.

Data Availability Statement

The data that support the findings of this study are available from the corresponding author upon reasonable request.

Keywords: Hyperpolarization · Metabolic Imaging · Parahydrogen · Pyruvate · SABRE

[1] E. A. Eisenhauer, P. Therasse, J. Bogaerts, L. H. Schwartz, D. Sargent, R. Ford, J. Dancey, S. Arbuck, S. Gwyther, M. Mooney, L. Rubinstein, L. Shankar, L. Dodd, R. Kaplan, D. Lacombe, J. Verweij, *Eur. J. Cancer* **2009**, *45*, 228–247.

[2] S. E. Day, M. I. Kettunen, F. A. Gallagher, D.-E. Hu, M. Lerche, J. Wolber, K. Golman, J. H. Ardenkjaer-Larsen, K. M. Brindle, *Nat. Med.* **2007**, *13*, 1382–1387.

[3] Z. J. Wang, M. A. Ohliger, P. E. Larson, J. W. Gordon, R. A. Bok, J. Slater, J. E. Villanueva-Meyer, C. P. Hess, J. Kurhanewicz, D. B. Vigneron, *Radiology* **2019**, *291*, 273.

[4] J. Kurhanewicz, D. B. Vigneron, J. H. Ardenkjaer-Larsen, J. A. Bankson, K. Brindle, C. H. Cunningham, F. A. Gallagher, K. R. Keshari, A. Kjaer, C. Laustsen, D. A. Mankoff, M. E. Merritt, S. J. Nelson, J. M. Pauly, P. Lee, S. Ronen, D. J. Tyler, S. S. Rajan, D. M. Spielman, L. Wald, X. Zhang, C. R. Malloy, R. Rizi, *Neoplasia* **2019**, *21*, 1–16.

[5] R. Woitek, M. A. McLean, S. Ursprung, O. M. Rueda, R. Manzano Garcia, M. J. Locke, L. Beer, G. Baxter, L. Rundo, E. Provenzano, J. Kaggie, A. Patterson, A. Frary, J. Field-Rayner, V. Papalouka, J. Kane, A. J. V. Benjamin, A. B. Gill, A. N. Priest, D. Y. Lewis, R. Russell, A. Grimmer, B. White, B. Latimer-Bowman, I. Patterson, A. Schiller, B. Carmo, R. Slough, T. Lanz, J. Wason, R. F. Schulte, S.-F. Chin, M. J. Graves, F. J. Gilbert, J. E. Abraham, C. Caldas, K. M. Brindle, E. Sala, F. A. Gallagher, *Cancer Res.* **2021**, *81*, 6004–6017.

[6] N. Sushentsev, M. A. McLean, A. Y. Warren, A. J. V. Benjamin, C. Brodie, A. Frary, A. B. Gill, J. Jones, J. D. Kaggie, B. W. Lamb, M. J. Locke, J. L. Miller, I. G. Mills, A. N. Priest, F. J. L. Robb, N. Shah, R. F. Schulte, M. J. Graves, V. J. Gnanapragasam, K. M. Brindle, T. Barrett, F. A. Gallagher, *Nat. Commun.* **2022**, *13*, 466.

[7] J.-H. Ardenkjaer-Larsen, G. S. Boebinger, A. Comment, S. Duckett, A. S. Edison, F. Engelke, C. Griesinger, R. G. Griffin, C. Hilty, H. Maeda, G. Parigi, T. Prisner, E. Ravera, J. van Bentum, S. Vega, A. Webb, C. Luchinat, H. Schwalbe, L. Frydman, *Angew. Chem. Int. Ed.* **2015**, *54*, 9162–9185.

[8] J. H. Ardenkjær-Larsen, S. Bowen, J. R. Petersen, O. Rybalko, M. S. Vinding, M. Ullisch, N. Chr Nielsen, *Magn. Reson. Med.* **2019**, *81*, 2184–2194.

[9] A. Capozzi, T. Cheng, G. Boero, C. Roussel, A. Comment, *Nat. Commun.* **2017**, *8*, 15757.

[10] S. Jannin, A. Bornet, R. Melzi, G. Bodenhausen, *Chem. Phys. Lett.* **2012**, *549*, 99–102.

[11] F. Reineri, E. Cavallari, C. Carrera, S. Aime, *Magn. Reson. Mater. Phys. Biol. Med.* **2021**, *34*, 25–47.

[12] A. B. Schmidt, C. R. Bowers, K. Buckenmaier, E. Y. Chekmenev, H. de Maissin, J. Eills, F. Ellermann, S. Glöggler, J. W. Gordon, S. Knecht, I. V. Koptyug, J. Kuhn, A. N. Pravdivtsev, F. Reineri, T. Theis, K. Them, J.-B. Hövener, *Anal. Chem.* **2022**, *94*, 479–502.

[13] P. Saul, L. Schröder, A. B. Schmidt, J.-B. Hövener, *WIREs Nanomed. Nanobiotechnol.* **2023**, *15*, e1879.

[14] J. Eills, D. Budker, S. Cavagnero, E. Y. Chekmenev, S. J. Elliott, S. Jannin, A. Lesage, J. Matysik, T. Meersmann, T. Prisner, J. A. Reimer, H. Yang, I. V. Koptyug, *Chem. Rev.* **2023**, *123*, 1417–1551.

[15] F. Reineri, T. Boi, S. Aime, *Nat. Commun.* **2015**, *6*, 5858.

[16] R. W. Adams, J. A. Aguilar, K. D. Atkinson, M. J. Cowley, P. I. P. Elliott, S. B. Duckett, G. G. R. Green, I. G. Khazal, J. López-Serrano, D. C. Williamson, *Science* **2009**, *323*, 1708–1711.

[17] T. Theis, M. L. Truong, A. M. Coffey, R. V. Shchepin, K. W. Waddell, F. Shi, B. M. Goodson, W. S. Warren, E. Y. Chekmenev, *J. Am. Chem. Soc.* **2015**, *137*, 1404–1407.

[18] V. V. Zhivonitko, I. V. Skovpin, I. V. Koptyug, *Chem. Commun.* **2015**, *51*, 2506–2509.

[19] A. N. Pravdivtsev, A. V. Yurkovskaya, H. Zimmermann, H.-M. Vieth, K. L. Ivanov, *Chem. Phys. Lett.* **2016**, *661*, 77–82.

[20] S. Knecht, A. S. Kiryutin, A. V. Yurkovskaya, K. L. Ivanov, *J. Magn. Reson.* **2018**, *287*, 10–14.

[21] J. R. Lindale, S. L. Eriksson, C. P. N. Tanner, Z. Zhou, J. F. P. Colell, G. Zhang, J. Bae, E. Y. Chekmenev, T. Theis, W. S. Warren, *Nat. Commun.* **2019**, *10*, 395.

[22] S. L. Eriksson, J. R. Lindale, X. Li, W. S. Warren, *Sci. Adv.* **2022**, *8*, eabl3708.

[23] W. Iali, S. S. Roy, B. J. Tickner, F. Ahwal, A. J. Kennerley, S. B. Duckett, *Angew. Chem.* **2019**, *131*, 10377–10381.

[24] P. TomHon, M. Abdulmojeed, I. Adelabu, S. Nantogma, M. S. H. Kabir, S. Lehmkuhl, E. Y. Chekmenev, T. Theis, *J. Am. Chem. Soc.* **2022**, *144*, 282–287.

[25] I. Adelabu, P. TomHon, M. S. H. Kabir, S. Nantogma, M. Abdulmojeed, I. Mandzhieva, J. Ettedgui, R. E. Swenson, M. C. Krishna, T. Theis, B. M. Goodson, E. Y. Chekmenev, *ChemPhysChem* **2022**, *23*, e202100839.

[26] S. Nantogma, S. L. Eriksson, I. Adelabu, I. Mandzhieva, A. Browning, P. TomHon, W. S. Warren, T. Theis, B. M. Goodson, E. Y. Chekmenev, *J. Phys. Chem. A* **2022**, *126*, 9114–9123.

[27] A. B. Schmidt, H. de Maissin, I. Adelabu, S. Nantogma, J. Ettedgui, P. TomHon, B. M. Goodson, T. Theis, E. Y. Chekmenev, *ACS Sens.* **2022**, *7*, 3430–3439.

[28] J.-B. Hövener, N. Schwaderlapp, R. Borowiak, T. Lickert, S. B. Duckett, R. E. Mewis, R. W. Adams, M. J. Burns, L. A. R. Highton, G. G. R. Green, A. Olaru, J. Hennig, D. von Elverfeldt, *Anal. Chem.* **2014**, *86*, 1767–1774.

[29] J. F. P. Colell, M. Emondts, A. W. J. Logan, K. Shen, J. Bae, R. V. Shchepin, G. X. Ortiz, P. Spannring, Q. Wang, S. J. Malcolmson, E. Y. Chekmenev, M. C. Feiters, F. P. J. T. Rutjes, B. Blümich, T. Theis, W. S. Warren, *J. Am. Chem. Soc.* **2017**, *139*, 7761–7767.

[30] P. Spannring, I. Reile, M. Emondts, P. P. M. Schleker, N. K. J. Hermkens, N. G. J. van der Zwaluw, B. J. A. van Weerdenburg, P. Tinnemans, M. Tessari, B. Blümich, F. P. J. T. Rutjes, M. C. Feiters, *Chem. Eur. J.* **2016**, *22*, 9277–9282.

[31] D. A. Barskiy, L. A. Ke, X. Li, V. Stevenson, N. Widarman, H. Zhang, A. Truxal, A. Pines, *J. Phys. Chem. Lett.* **2018**, *9*, 2721–2724.

[32] B. E. Kidd, J. L. Gesiorski, M. E. Gemeinhardt, R. V. Shchepin, K. V. Kovtunov, I. V. Koptyug, E. Y. Chekmenev, B. M. Goodson, *J. Phys. Chem. C* **2018**, *122*, 16848–16852.

[33] S. J. DeVience, R. L. Walsworth, M. S. Rosen, *Phys. Rev. Lett.* **2013**, *111*, 173002.

[34] T. Theis, M. Truong, A. M. Coffey, E. Y. Chekmenev, W. S. Warren, *J. Magn. Reson.* **2014**, *248*, 23–26.

[35] A. N. Pravdivtsev, K. Buckenmaier, N. Kempf, G. Stevanato, K. Scheffler, J. Engelmann, M. Plaumann, R. Koerber, J.-B. Hövener, T. Theis, *J. Phys. Chem. C* **2023**, *127*, 6744–6753.

[36] A. B. Schmidt, J. Eills, L. Dagys, M. Gierse, M. Keim, S. Lucas, M. Bock, I. Schwartz, M. Zaitsev, E. Y. Chekmenev, S. Knecht, *J. Phys. Chem. Lett.* **2023**, *14*, 5305–5309.
[37] Y. Ding, S. Korchak, S. Mamone, A. P. Jagtap, G. Stevanato, S. Sternkopf, D. Moll, H. Schroeder, S. Becker, A. Fischer, E. Gerhardt, T. F. Outeiro, F. Opazo, C. Griesinger, S. Glöggler, *Chem. Methods* **2022**, *2*, e202200023.
[38] J. G. Skinner, G. J. Topping, L. Nagel, I. Heid, C. Hundshammer, M. Grashei, F. H. A. van Heijster, R. Braren, F. Schilling, *Magn. Reson. Med.* **2023**, *90*, 894–909.
[39] J.-B. Hövener, N. Schwaderlapp, T. Lickert, S. B. Duckett, R. E. Mewis, L. A. R. Highton, S. M. Kenny, G. G. R. Green, D. Leibfritz, J. G. Korvink, J. Hennig, D. von Elverfeldt, *Nat. Commun.* **2013**, *4*, 2946.
[40] A. B. Schmidt, M. Zimmermann, S. Berner, H. de Maissin, C. A. Müller, V. Ivantaev, J. Hennig, D. v Elverfeldt, J.-B. Hövener, *Commun. Chem.* **2022**, *5*, 21.
[41] A. M. Funk, X. Wen, T. Hever, N. R. Maptue, C. Khemtong, A. D. Sherry, C. R. Malloy, *J. Magn. Reson.* **2019**, *301*, 102–108.
[42] A. Ferrari, J. Peters, M. Anikeeva, A. Pravdivtsev, F. Ellermann, K. Them, O. Will, E. Peschke, H. Yoshihara, O. Jansen, J.-B. Hövener, *Sci. Rep.* **2022**, *12*, 11694.
[43] A. Duchowny, J. Denninger, L. Lohmann, T. Theis, S. Lehmkuhl, A. Adams, *Int. J. Mol. Sci.* **2023**, *24*, 2465.
[44] A. B. Schmidt, S. Berner, M. Braig, M. Zimmermann, J. Hennig, D. von Elverfeldt, J.-B. Hövener, *PLoS One* **2018**, *13*, e0200141.
[45] S. Berner, A. B. Schmidt, F. Ellermann, S. Korchak, E. Y. Chekmenev, S. Glöggler, D. von Elverfeldt, J. Hennig, J.-B. Hövener, *Phys. Chem. Chem. Phys.* **2021**, *23*, 2320–2330.
[46] PubChem, "Methanol," can be found under https://pubchem.ncbi.nlm.nih.gov/compound/887.
[47] B. Mégarbane, *Open Access Emerg. Med. OAEM* **2010**, *2*, 67–75.
[48] ICH HARMONISED GUIDELINE Q3C(R8), **2021**.
[49] ICH HARMONISED GUIDELINE Q3D(R2), **2022**.
[50] J.-B. Hövener, S. Bär, J. Leupold, K. Jenne, D. Leibfritz, J. Hennig, S. B. Duckett, D. von Elverfeldt, *NMR Biomed.* **2013**, *26*, 124–131.
[51] R. Savka, H. Plenio, *Dalton Trans.* **2015**, *44*, 891–893.
[52] A. B. Schmidt, D. L. Andrews, A. Rohrbach, C. Gohn-Kreuz, V. N. Shatokhin, V. G. Kiselev, J. Hennig, D. von Elverfeldt, J.-B. Hövener, *J. Magn. Reson.* **2016**, *268*, 58–67.
[53] A. S. Kiryutin, G. Sauer, S. Hadjiali, A. V. Yurkovskaya, H. Breitzke, G. Buntkowsky, *J. Magn. Reson.* **2017**, *285*, 26–36.
[54] H. Wolinsky, S. Glagov, *Circ. Res.* **1967**, *20*, 99–111.
[55] S. J. Nelson, J. Kurhanewicz, D. B. Vigneron, P. E. Z. Larson, A. L. Harzstark, M. Ferrone, M. van Criekinge, J. W. Chang, R. Bok, I. Park, G. Reed, L. Carvajal, E. J. Small, P. Munster, V. K. Weinberg, J. H. Ardenkjaer-Larsen, A. P. Chen, R. E. Hurd, L.-I. Odegardstuen, F. J. Robb, J. Tropp, J. A. Murray, *Sci. Transl. Med.* **2013**, *5*, 108.
[56] K. MacCulloch, A. Browning, D. O. Guarin Bedoya, S. J. McBride, M. B. Abdulmojeed, C. Dedesma, B. M. Goodson, M. S. Rosen, E. Y. Chekmenev, Y.-F. Yen, P. TomHon, T. Theis, *J. Magn. Reson. Open* **2023**, *16–17*, 100129 https://doi.org/10.1016/j.jmro.2023.100129.

Manuscript received: March 27, 2023
Accepted manuscript online: July 13, 2023
Version of record online: July 25, 2023